THE JOURNAL OF PHYSICAL CHEMISTRY Letters

Letter

pubs.acs.org/JPCL

Irreversible Adsorption Controls Crystallization in Vapor-Deposited Polymer Thin Films

Hyuncheol Jeong,[†] Simone Napolitano,[§] Craig B. Arnold,[‡,⊥] and Rodney D. Priestley*[,†,⊥]

[†]Department of Chemical and Biological Engineering, Princeton University, Princeton, New Jersey 08544, United States

[§]Laboratory of Polymer and Soft Matter Dynamics, Faculté des Sciences, Université Libre de Bruxelles (ULB), Bruxelles 1050, Belgium

[‡]Department of Mechanical and Aerospace Engineering, Princeton University, Princeton, New Jersey 08544, United States

[⊥]Princeton Institute for the Science and Technology of Materials, Princeton University, Princeton, New Jersey 08544, United States

ABSTRACT: Matrix-assisted pulsed laser evaporation (MAPLE) provides a gentle means for the quasi-vapor deposition of macromolecules. It offers a unique opportunity for the bottom-up control of polymer crystallization as film growth and crystallization occur simultaneously. Surprisingly, with increasing deposition time, it has been shown that crystallization becomes prohibited despite the availability of polymer via continuous deposition. In this Letter, we investigate the molecular origins of suppressed crystallization in poly(ethylene oxide) films deposited by MAPLE atop silicon substrates. We find that suppressed crystallization results from the formation of an irreversibly adsorbed polymer nanolayer at the substrate that forms during deposition. Substrate temperature is shown to influence the stability of the irreversibly adsorbed nanolayer and, hence, polymer thin film crystallization. Our investigation offers new insight into how temperature and interfacial interactions can serve as a new toolbox to tune polymer film morphology in bottom-up deposition.

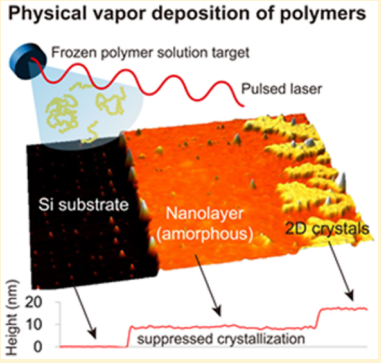

The bottom-up deposition of thin films in which molecular-scale film growth and crystallization occur simultaneously is highly desirable as the influence of interfaces on nucleation and growth can be exploited during processing to control film morphology.[1,2] In such a process, slow growth rates facilitate molecular ordering of the deposited material, while other process parameters, for example, substrate surface properties and temperature, may be exploited to tune molecular mobility and hence manipulate morphology. In the case of atomic and molecular systems, physical vapor deposition (PVD) has been successfully employed as a bottom-up approach to control the characteristics of thin films, including the morphology and thickness.[1−4] Achieving similar control of morphology in polymer films represents a major challenge via PVD because their high molecular weights (>500 g/mol) have previously precluded their direct and additive deposition with this approach.

The development of matrix-assisted pulsed laser evaporation (MAPLE), which provides a gentle means for the deposition of high molecular polymers from the near-gas-phase growth conditions,[5−10] offers a unique opportunity for bottom-up polymer film growth to control morphology. For instance, it has been shown that MAPLE can be used to control preferential crystal orientation and the extent of crystallinity in polymer thin films by adjusting the matrix formulation[11] and substrate temperature,[12] respectively. Recently, we demonstrated the sequential growth and crystallization of polymer thin films deposited via MAPLE at slow growth rates.[13] We found that the MAPLE of poly(ethylene oxide) (PEO) atop silicon (Si) substrates held at a substrate temperature (T_{sub}) well below the melting point (T_m) of PEO led to the formation of two-dimensional (2D) crystals during deposition, composed of monolamellar crystals laterally grown from larger nucleating droplets. Surprisingly, as the deposition time increased beyond a certain value, the 2D crystal growth atop the Si substrate ceased despite the availability of amorphous PEO at the 2D crystal growth front. Qualitatively, the suppressed crystallization of MAPLE-deposited PEO (MAPLE PEO) could be rationalized by suggesting that the amorphous PEO is stable against crystallization.

Inspired by our recent report, in this Letter, we investigate the origins of the suppressed crystallization of MAPLE-deposited films and demonstrate a means of tuning the film's morphology. We demonstrate that substrate temperature during deposition strongly impacts the ability of MAPLE-deposited films to undergo crystallization. By measuring the thickness of an irreversibly adsorbed nanolayer formed during film formation, as a function of deposition temperature, we document that its presence strongly influences whether films deposited via MAPLE undergo extensive crystallization or whether ordering is suppressed during film growth. Considering that MAPLE represents an emerging and unique platform for polymer film deposition, combined with limited fundamental understanding of how MAPLE processing influences

Received: November 3, 2016
Accepted: December 15, 2016
Published: December 15, 2016

DOI: 10.1021/acs.jpclett.6b02573
J. Phys. Chem. Lett. 2017, 8, 229−234

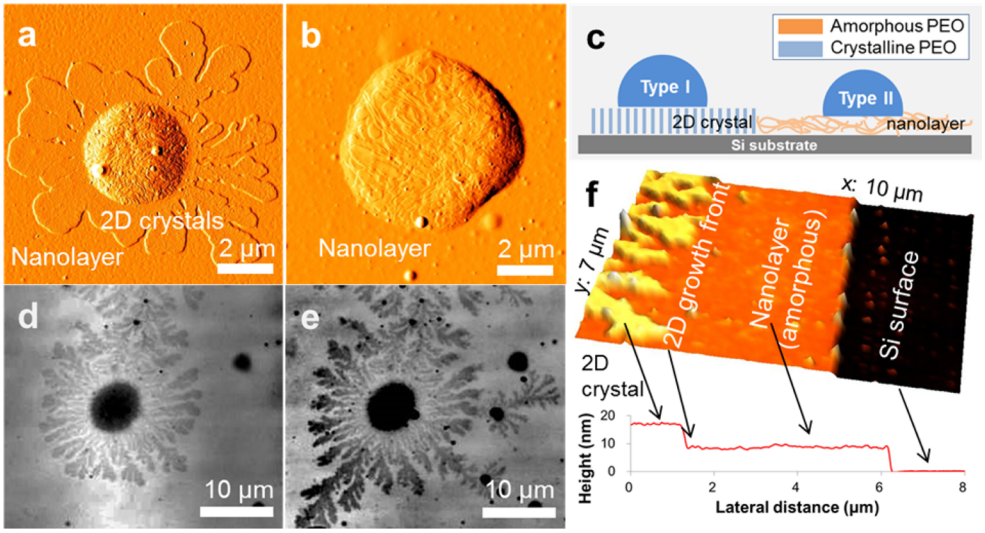

Figure 1. (a,b) AFM amplitude images showing two types of crystalline microdroplets deposited during MAPLE at T_{sub} = 25 °C. (a) Type I microdroplet with surrounding 2D crystals; (b) type II microdroplet without 2D crystals. (c) Schematic showing the structure of type I and II droplets. (d,e) Optical microscopy images taken with a 405 nm laser showing the growth of 2D crystals after additive PEO deposition; (d) taken after the first 2 h of MAPLE at T_{sub} = 25 °C (M1) and (e) taken after another 2 h of the second MAPLE (M2). (f) AFM height image showing the morphology of the MAPLE PEO film formed with t_{dep} = 6 h (upper panel) and the corresponding AFM height profile (lower panel). Dendritic 2D crystals, a surrounding nanolayer, and an area scraped with a razor blade (Si surface) are depicted. No depletion zone exists between the 2D crystal growth front and the contacting nanolayer.

morphology, this investigation offers new insight into how substrate temperature and interfacial interactions can serve as a new toolbox to tune film morphology.

Conceptually, MAPLE proceeds by the additive deposition of a size distribution of polymer droplets.[14] In the case of PEO deposited atop Si, the larger droplets self-nucleate and act as centers for dendritic 2D crystal growth. Smaller droplets either crystallize into 2D crystals via epitaxial growth from the nuclei or spread atop the surface and remain amorphous, forming an amorphous nanolayer.[13] While this mechanism is remarkably similar to the crystallization of metals and molecular compounds deposited via PVD,[4,15] the resulting morphologies of the monolayers are in stark contrast due to suppressed crystallization in the nanolayer that remains amorphous in MAPLE PEO films.

To understand the origins of the suppressed crystallization in MAPLE PEO films, we began by investigating the growth of 2D crystals from droplets of diameter D > 2.5 μm (microdroplets) as a function of deposition time (t_{dep}). We conducted three sequential MAPLE depositions (M1, M2, and M3), each with 2 h intervals at T_{sub} = 25 °C, on the same film and analyzed the morphology of the microdroplets formed at each time interval. The crystalline microdroplets exhibited two types of morphologies: type I, in which the crystalline droplet is surround by 2D crystals, or type II, in which the crystalline droplet is surround by an amorphous nanolayer. The two representative crystalline microdroplet morphologies are imaged by AFM in Figure 1a,b, respectively, and illustrated schematically in Figure 1c.

Table 1 presents an analysis of the crystalline microdroplet morphology at the three different time intervals, M1, M2, and M3. For t_{dep} = 0−2 h, that is, during M1, 96% of the crystalline droplets formed exhibited a type I morphology, while for t_{dep} = 2−4 h, that is, during M2, 75% of the crystalline droplets formed exhibited a type I morphology. Strikingly, for t_{dep} = 4−6 h, that is, during M3, 0% of the crystalline droplets formed exhibited type I morphology. This interval-resolved morphology analysis revealed several important observations: (i) nearly all nucleating microdroplets initiated 2D crystal growth in the early stages of film formation, and (ii) as t_{dep} increased, the ability of the nucleating droplets to initiate 2D crystal growth diminished.

Table 1. Analysis of the Morphology of Crystalline Microdroplets (D > 2.5 μm) and 2D Growth during Three Sequential MAPLE (MP) Depositions[a]

droplets of interest	first MP	second MP	third MP
type I droplets among crystalline droplets	0.96	0.75	0
first MP crystalline droplets with 2D growth	n/a	0.62	0

[a]The first row shows the ratio of type I droplets among all crystalline droplets formed at each different deposition. The second row shows the ratio of the first MP crystalline droplets that developed detectable 2D growth (> 2.5 μm) at the second and third MPs.

As t_{dep} increased, so did the thickness of the amorphous nanolayer on the substrate, with a growth rate of ∼1.5 nm/h. Hence, while the crystalline microdroplets formed during M1 were deposited atop a nanolayer of thickness 0−3 nm, those formed during M3 were deposited atop a nanolayer of thickness 6−9 nm. In considering this difference, we argue that the presence of a thick underlying PEO nanolayer prevents the microdroplets from nucleating 2D crystals during the later stages of film growth and, thus, suppresses the overall crystallization. This is an important observation as it hints to a possible fundamental limitation in the gas-phase deposition of macromolecules.

Furthermore, we analyzed whether 2D crystals formed during M1 exhibited additional growth due the continued deposition of PEO during later deposition intervals. Figure 1d,e compares the morphology of the same 2D crystalline island after M1 and M2, respectively, showing the growth of 2D crystals during M2. As shown in Table 1, of the 2D crystalline islands formed during M1, only 62% exhibited additional 2D

DOI: 10.1021/acs.jpclett.6b02573
J. Phys. Chem. Lett. 2017, 8, 229−234

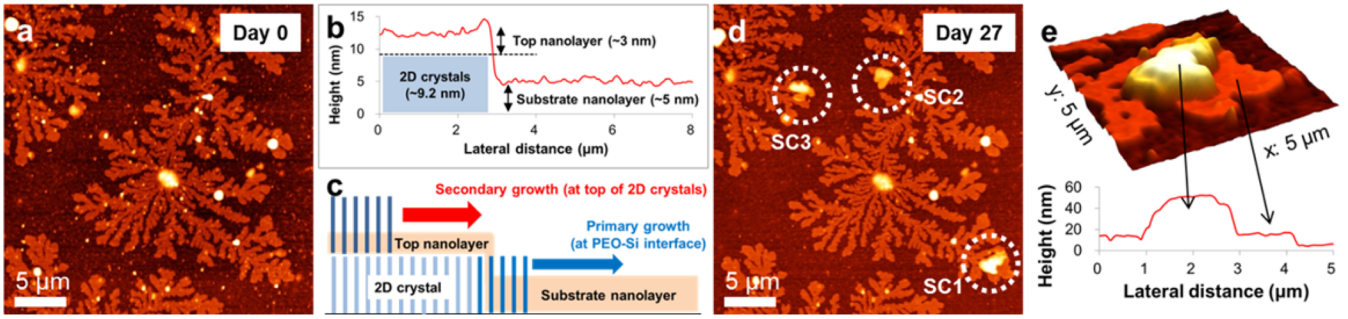

Figure 2. (a) AFM height image of an as-deposited MAPLE PEO film made with T_{sub} = 25 °C and t_{dep} = 3 h. (b) AFM height profile of the MAPLE PEO film in panel (a). The profile depicts ~9.2 nm thick 2D crystals, a ~3 nm top nanolayer deposited atop the 2D crystals, and a ~5 nm substrate nanolayer atop the Si surface. (c) Schematic showing two possible cases of 2D crystal growth in MAPLE PEO films upon aging. The blue arrow describes primary growth, continuing from the lateral faces of 2D crystals. The red arrow describes secondary growth, growing from the fold surfaces of the 2D crystals. (d) AFM height image of the film in panel (a) taken after 27 days of aging at 25 °C under a N_2 environment. White dashed circles depict three secondary crystals (SC1−3) formed during aging. (e) AFM height image magnifying SC1 in panel (d) (upper panel) and the corresponding height profile (lower panel).

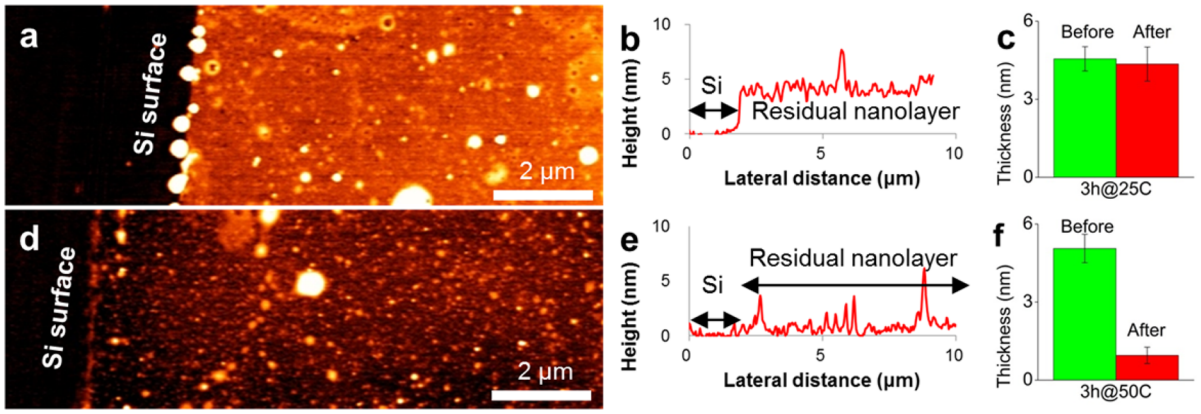

Figure 3. AFM height image (a) and AFM profile (b) of a substrate nanolayer in a 3h@25C film, after 20 min of toluene washing. (c) Graph comparing the nanolayer thickness in a 3h@25C film before and after toluene washing. AFM height image (d) and AFM profile (e) of a substrate nanolayer in a 3h@50C film, after 20 min of toluene washing. (f) Graph comparing the substrate nanolayer thickness in a 3h@50C film before and after toluene washing.

growth during M2, and no additional growth was exhibited during M3. In this case, the lateral faces as well as the fold surfaces of the 2D crystals were surrounded by an amorphous nanolayer with no evidence of a depletion zone at the crystal growth front, as illustrated in Figure 1f. Remarkably, the amorphous PEO in direct contact with the crystal surface is stable against crystallization. These findings further illustrate the suppressed growth of 2D crystals as t_{dep} increases. More importantly, they corroborate the idea that as the thickness of the amorphous PEO nanolayer grows, with increasing t_{dep}, growth of 2D crystals is suppressed.

To investigate the long-term stability of the nanolayer against crystallization, we monitored the morphology of a PEO film, deposited at T_{sub} = 25 °C atop Si, during aging. Figure 2a shows the representative AFM morphology of the film directly after 3 h of deposition at 25 °C in which both 2D crystals and a nanolayer are present. The ~10 nm thick 2D crystals, formed at an early stage of deposition, are covered with a ~3 nm PEO nanolayer deposited afterward. The nanolayer atop the Si, which contacts with the lateral faces of the 2D crystals, is approximately 5 nm thick. Figure 2b shows an AFM profile image that confirms these film dimensions. We aged the film under N_2 at 25 °C for 27 days to determine if the morphology evolved with time. More specifically, we wanted to determine whether amorphous PEO in the nanolayer transformed into the crystalline phase from the lateral faces of the 2D crystals (primary growth, see Figure 2c) or from the top of the 2D crystals (secondary growth, see Figure 2c), both of which are expected from an epitaxial growth mechanism.[16−19] Surprisingly, the film morphology taken after 27 days of aging (see Figure 2d) indicates that the 2D crystals showed no evidence of primary growth from the nanolayer at the Si interface (substrate nanolayer) during the prolonged annealing period well below T_m. In essence, the substrate nanolayer is stable against crystallization and therefore does not allow for the growth of 2D crystals in lateral dimensions. In contrast, evidence of secondary growth from the nanolayer atop 2D crystals (top nanolayer) was observed to a limited extent, as illustrated by the dotted circles (SC1−3) in Figure 2d. Figure 2e shows an AFM height and profile image of a crystal SC1 in Figure 2d, formed by a secondary growth event. Thus, while the substrate nanolayer at Si has no mobility for further crystallization, the nanolayer atop the 2D crystals had sufficient mobility for crystallization.

To better understand the origins of the suppressed crystallization, we focused on obtaining evidence of strong PEO nanolayer−substrate interactions. Suppressed crystal growth in thin films has been associated with reductions of the mobility of chains in the uncrystallized fraction.[20,21] In thin amorphous polymer films, such reduction of chain mobility can

DOI: 10.1021/acs.jpclett.6b02573
J. Phys. Chem. Lett. 2017, 8, 229−234

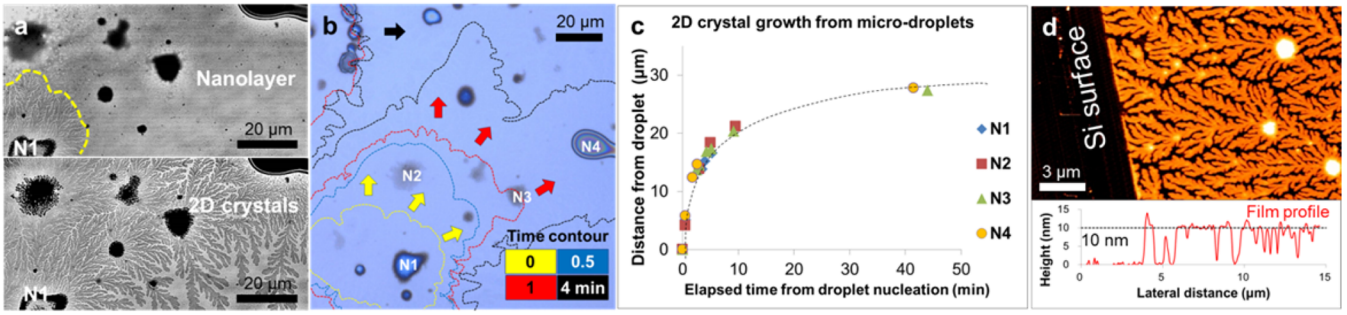

Figure 4. (a) Optical microscopy images taken with a 405 nm laser showing 2D crystal growth from a MAPLE PEO film during aging at 25 °C. The film was made with T_{sub} = 50 °C and t_{dep} = 3 h and quickly transferred onto a 25 °C temperature stage. The upper panel was captured right after crystallization in droplet N1, and the lower panel was captured after 1 h of aging; (b) propagation of 2D crystal growth as a function of time. (c) Plots showing 2D crystal growth from four microdroplets (N1−N4) in panel (b). The radial 2D crystal growth from each droplet is plotted as a function of time elapsed from the point of droplet crystallization. (d) AFM height image (upper panel) showing 2D crystals grown from the substrate nanolayer during aging. The left side of the film was scraped with a razor blade. The measured height of the 2D crystals was ∼10 nm, as depicted in the lower panel.

occur due to pinning of chain segments onto the substrate that forms irreversibly adsorbed layers (IALs).[22−24] We reason that the development of an IAL at the nanolayer−Si surface suppresses crystal growth. To establish the existence of an IAL, following Guiselin's experiment,[25−29] we measured the residual substrate nanolayer thickness after solvent washing of a MAPLE PEO film formed with T_{sub} = 25 °C and t_{dep} = 3 h, that is, 3h@25C MAPLE. The methodology is a well-established technique to uncover loosely adsorbed chains in polymer films; therefore, residual film thickness can be the indicator of the degree of adsorption. Solvent washing was done by dipping the films into toluene for 20 min. Figure 3a,b shows an AFM height image and a representative AFM profile of a residual substrate nanolayer after solvent washing, respectively. Figure 3c compares the average substrate nanolayer thickness before and after solvent washing. Clearly, solvent washing did not modify the original thickness (∼5 nm), thus indicating the presence of a strongly bound IAL.

As the mobility of polymer chains critically depends on temperature, we next sought to investigate the effect of a higher T_{sub} close to T_m, at which the deposited PEO chains would have a higher kinetic energy and thus higher desorption probability. We therefore deposited a PEO film at T_{sub} = 50 °C for t_{dep} = 3 h, that is, 3h@50C MAPLE. Solvent washing was performed for 20 min after equilibrating the as-deposited 3h@50C sample at 25 °C for 5 min. Figure 3d,e shows an AFM height image and a representative AFM profile of a solvent-washed residual substrate nanolayer, respectively, and Figure 3d compares the average substrate nanolayer thickness before and after solvent washing. Noticeably, the film thickness dramatically decreased from ∼5 to ∼1 nm after solvent washing. As shown by the profile spectrum in Figure 3e, we can firmly conclude that deposition at higher T_{sub} reduces the development of an IAL during MAPLE.

On the basis of these findings, we next evaluated the morphological development of the 3h@50C MAPLE PEO film during aging. The as-deposited 3h@50C sample was readily transferred to the 25 °C temperature stage and monitored under optical microscopy to provide the same aging environment as that in the case of the 3h@25C sample above. As this high T_{sub} (50 °C) effectively suppresses crystal nucleation of PEO, the majority of the film would remain uncrystallized during deposition and only become able to nucleate when moved onto the 25 °C stage.[13] Figure 4a compares a film morphology right after crystallization of the N1 droplet (see the upper panel) at 25 °C and the morphology of the same region captured after 1 h (see the lower panel). It is obvious that the crystal growth propagated through the nanolayer region, forming dendritic 2D crystals. Such crystal growth propagated into the entire substrate region of ∼2 cm^2 once nucleation events occurred. Figure 4b is an optical microscopy image of the sample in Figure 4a, with time contours showing the location of the crystal growth front at times 0 (yellow line), 0.5 (blue), 1 (red), and 4 min (black). The propagation of the 2D growth crystallized microdroplets N1−N4 in the order named. Figure 4c plots the 2D crystal growth from the four microdroplets in Figure 4b, N1−N4 respectively, as a function of time. In the respective growth plots, the time of crystallization of the corresponding droplets was set to zero. They all collapsed in one line, indicated as a black dashed curve, showing retarded growth rate as they grow farther away from the microdroplet. Finally, Figure 4d exhibits the AFM morphology of 2D crystals of the 3h@50C sample after crystallization. The ∼10 nm thickness of the 2D crystals is identical to the thickness of the crystals formed via MAPLE at T_{sub} = 25 °C.

Interestingly, MAPLE deposition at T_{sub} = 50 °C renders primary growth from the ∼5 nm thick nanolayer at 25 °C, as opposed to the case of the nanolayer with comparable thickness and aging temperature but formed at T_{sub} = 25 °C. The findings corroborate the notion that suppressed crystallization during MAPLE is due to the development of an IAL during deposition. Irreversible adsorption of chains can lead to a reduction or complete suppression of crystallization as there is a high entropic barrier required for reorganization of chains from IAL.[21,30] From this point of view, we conclude that while the strongly bound substrate nanolayer of ∼5 nm in 3h@25C samples prohibits primary growth, the loosely adsorbed nanolayer in 3h@50C allows the growth of primary MLCs once nucleation events occur.

In summary, we investigated crystal growth in vapor-deposited PEO films and provided evidence that the deposition temperature in MAPLE of polymers can affect the stability of deposited polymer thin films against crystallization. In a PEO film deposited at 25 °C, the uncrystallized fraction of the PEO was strongly adsorbed to the Si surface and resistant to crystallization during 25 °C aging. However, when the deposition was performed at 50 °C, the adsorption of the

DOI: 10.1021/acs.jpclett.6b02573
J. Phys. Chem. Lett. 2017, 8, 229−234

uncrystallized PEO fraction to Si was dramatically lessened and exhibited rapid crystal growth during 25 °C aging. Our results imply that the deposition temperature combined with interfacial interactions can define the nature of deposited thin polymer films in MAPLE processing, and the thermal history of polymer thin films can affect the crystallization kinetics. Future work will seek to demonstrate how MAPLE deposition atop substrates with different properties can be used to control thin film morphology.

EXPERIMENTAL METHODS

Details of the MAPLE deposition of PEO were described in our previous study.[13] The deposition of PEO (M_n = 4600 g/mol, polydispersity = 1.1) onto as-received Si substrates was achieved by laser ablation from a frozen MAPLE target, where PEO was dissolved in dimethyl sulfoxide at a concentration of 1 mg/mL. The laser ablation was conducted in a vacuum environment using a KrF laser (LightMachinery PulseMaster 844, λ = 248 nm, pulse duration = 20 ns). The laser was operated with a repetition rate of 5 Hz and energy of 13.5−14.0 mJ/pulse with the focal area of 15 mm^2.

For solvent washing, the MAPLE PEO sample of interest was cut into ∼0.5 cm × 2 cm sheets and then vertically soaked in toluene (20 mL volume glass vial) at room temperature. After submersion for 20 min, the sample was taken out, briefly rinsed with fresh toluene, blown with N_2, and dried in a vacuum oven at room temperature. Three different regions of the film were investigated via AFM to obtain the average thickness of a substrate nanolayer before and after solvent washing.

For AFM measurements, a tapping mode AFM (Asylum Research MFP-3D-SA) was used for imaging. AFM image processing and analysis were performed using Gwyddion software. The thickness of a nanolayer in MAPLE PEO films was determined by measuring the height of steps obtained by removing the MAPLE-deposited area with a razor blade. Only flat film areas having no microdroplets atop were considered in measuring the nanolayer thickness. The root-mean-square roughness of a substrate nanolayer formed with 3 h of MAPLE was typically below 1 nm.

For optical microscopy measurements, a laser scanning confocal microscope (Olympus OLS4000), equipped with white light and a 405 nm laser as a light source, was used for imaging. The images taken with the 405 nm laser were processed to enhance contrast and brightness. A film area of ∼1.53 × 10^5 μm^2 was investigated for the analysis of 2D crystal growth as well as the morphology of crystalline microdroplets at each time interval of sequential MAPLE depositions (M1−M3).

AUTHOR INFORMATION

Corresponding Author

*E-mail: rpriestl@princeton.edu.

ORCID

Rodney D. Priestley: 0000-0001-6765-2933

Notes

The authors declare no competing financial interest.

ACKNOWLEDGMENTS

R.D.P. and C.B.A. acknowledge support of the National Science Foundation (NSF) through a Materials Research Science and Engineering Center program through the Princeton Center for Complex Materials (DMR-1420541). R.D.P acknowledges the support of the AFOSR through a PECASE Award (FA9550-12-1-0223). H.J. acknowledges support from the Kwanjeong Educational Foundation in South Korea. S.N. acknowledges financial support from the Fonds de la Recherche Scientifique FNRS under Grant No. T.0147.16 "TIACIC."

REFERENCES

(1) Zhang, Z.; Lagally, M. G. Atomistic Processes in the Early Stages of Thin-Film Growth. *Science* **1997**, *276*, 377−383.
(2) Barth, J. V.; Costantini, G.; Kern, K. Engineering Atomic and Molecular Nanostructures at Surfaces. *Nature* **2005**, *437*, 671−679.
(3) Laudise, R. A.; Kloc, C.; Simpkins, P. G.; Siegrist, T. Physical Vapor Growth of Organic Semiconductors. *J. Cryst. Growth* **1998**, *187*, 449−454.
(4) Meyer zu Heringdorf, F.-J.; Reuter, M. C.; Tromp, R. M. Growth Dynamics of Pentacene Thin Films. *Nature* **2001**, *412*, 517−520.
(5) Piqué, A.; McGill, R. A.; Chrisey, D. B.; Leonhardt, D.; Mslna, T. E.; Spargo, B. J.; Callahan, J. H.; Vachet, R. W.; Chung, R.; Bucaro, M. A. Growth of Organic Thin Films by the Matrix Assisted Pulsed Laser Evaporation (MAPLE) Technique. *Thin Solid Films* **1999**, *355−356*, 536−541.
(6) Chrisey, D. B.; Piqué, A.; McGill, R. A.; Horwitz, J. S.; Ringeisen, B. R.; Bubb, D. M.; Wu, P. K. Laser Deposition of Polymer and Biomaterial Films. *Chem. Rev.* **2003**, *103*, 553−576.
(7) Leveugle, E.; Zhigilei, L. V. Molecular Dynamics Simulation Study of the Ejection and Transport of Polymer Molecules in Matrix-Assisted Pulsed Laser Evaporation. *J. Appl. Phys.* **2007**, *102*, 074914.
(8) Guo, Y.; Morozov, A.; Schneider, D.; Chung, J. W.; Zhang, C.; Waldmann, M.; Yao, N.; Fytas, G.; Arnold, C. B.; Priestley, R. D. Ultrastable Nanostructured Polymer Glasses. *Nat. Mater.* **2012**, *11*, 337−343.
(9) Shepard, K. B.; Priestley, R. D. MAPLE Deposition of Macromolecules. *Macromol. Chem. Phys.* **2013**, *214*, 862−872.
(10) Ge, W.; Li, N. K.; McCormick, R. D.; Lichtenberg, E.; Yingling, Y. G.; Stiff-Roberts, A. D. Emulsion-Based RIR-MAPLE Deposition of Conjugated Polymers: Primary Solvent Effect and Its Implications on Organic Solar Cell Performance. *ACS Appl. Mater. Interfaces* **2016**, *8*, 19494−19506.
(11) Liu, Y.; Atewologun, A.; Stiff-Roberts, A. D. Organic Semiconductor Thin Films Deposited by Resonant Infrared Matrix-Assisted Pulsed Laser Evaporation: A Fundamental Study of the Emulsion Target. *MRS Online Proc. Libr.* **2014**, *1733*, 957.
(12) Califano, V.; Bloisi, F.; Vicari, L.; Barra, M.; Cassinese, A.; Fanelli, E.; Buzio, R.; Valbusa, U.; Carella, A.; Roviello, A. Substrate Temperature Dependence of the Structure of Polythiophene Thin Films Obtained by Matrix Assisted Pulsed Laser Evaporation (MAPLE). *Eur. Phys. J.: Appl. Phys.* **2009**, *48*, 10505.
(13) Jeong, H.; Shepard, K. B.; Purdum, G. E.; Guo, Y.; Loo, Y.-L.; Arnold, C. B.; Priestley, R. D. Additive Growth and Crystallization of Polymer Films. *Macromolecules* **2016**, *49*, 2860−2867.
(14) Shepard, K. B.; Arnold, C. B.; Priestley, R. D. Origins of Nanostructure in Amorphous Polymer Coatings via Matrix Assisted Pulsed Laser Evaporation. *Appl. Phys. Lett.* **2013**, *103*, 123105.
(15) Hwang, R.; Schröder, J.; Günther, C.; Behm, R. Fractal Growth of Two-Dimensional Islands: Au on Ru(0001). *Phys. Rev. Lett.* **1991**, *67*, 3279−3282.
(16) Reiter, G.; Sommer, J.-U. Crystallization of Adsorbed Polymer Monolayers. *Phys. Rev. Lett.* **1998**, *80*, 3771−3774.
(17) Reiter, G. Some Unique Features of Polymer Crystallisation. *Chem. Soc. Rev.* **2014**, *43*, 2055−2065.
(18) Zhu, D.-S.; Liu, Y.-X.; Chen, E.-Q.; Li, M.; Chen, C.; Sun, Y.-H.; Shi, A.-C.; Van Horn, R. M.; Cheng, S. Z. D. Crystal Growth Mechanism Changes in Pseudo-Dewetted Poly(ethylene Oxide) Thin Layers. *Macromolecules* **2007**, *40*, 1570−1578.
(19) Zhang, H.; Yu, M.; Zhang, B.; Reiter, R.; Vielhauer, M.; Mülhaupt, R.; Xu, J.; Reiter, G. Correlating Polymer Crystals via Self-Induced Nucleation. *Phys. Rev. Lett.* **2014**, *112*, 237801.

DOI: 10.1021/acs.jpclett.6b02573
J. Phys. Chem. Lett. 2017, 8, 229−234

(20) Dalnoki-Veress, K.; Forrest, J. A.; Massa, M. V.; Pratt, A.; Williams, A. Crystal Growth Rate in Ultrathin Films of Poly(ethylene Oxide). *J. Polym. Sci., Part B: Polym. Phys.* **2001**, *39*, 2615−2621.
(21) Vanroy, B.; Wübbenhorst, M.; Napolitano, S. Crystallization of Thin Polymer Layers Confined between Two Adsorbing Walls. *ACS Macro Lett.* **2013**, *2*, 168−172.
(22) Koga, T.; Li, C.; Endoh, M. K.; Koo, J.; Rafailovich, M.; Narayanan, S.; Lee, D. R.; Lurio, L. B.; Sinha, S. K. Reduced Viscosity of the Free Surface in Entangled Polymer Melt Films. *Phys. Rev. Lett.* **2010**, *104*, 066101.
(23) Koga, T.; Jiang, N.; Gin, P.; Endoh, M. K.; Narayanan, S.; Lurio, L. B.; Sinha, S. K. Impact of an Irreversibly Adsorbed Layer on Local Viscosity of Nanoconfined Polymer Melts. *Phys. Rev. Lett.* **2011**, *107*, 225901.
(24) Jiang, N.; Sendogdular, L.; Di, X.; Sen, M.; Gin, P.; Endoh, M. K.; Koga, T.; Akgun, B.; Dimitriou, M.; Satija, S. Effect of CO_2 on a Mobility Gradient of Polymer Chains near an Impenetrable Solid. *Macromolecules* **2015**, *48*, 1795−1803.
(25) Guiselin, O. Irreversible Adsorption of a Concentrated Polymer Solution. *Europhys. Lett.* **1992**, *17*, 225−230.
(26) Fujii, Y.; Yang, Z.; Leach, J.; Atarashi, H.; Tanaka, K.; Tsui, O. K. C. Affinity of Polystyrene Films to Hydrogen-Passivated Silicon and Its Relevance to the T_g of the Films. *Macromolecules* **2009**, *42*, 7418−7422.
(27) Napolitano, S.; Wübbenhorst, M. The Lifetime of the Deviations from Bulk Behaviour in Polymers Confined at the Nanoscale. *Nat. Commun.* **2011**, *2*, 260.
(28) Gin, P.; Jiang, N.; Liang, C.; Taniguchi, T.; Akgun, B.; Satija, S. K.; Endoh, M. K.; Koga, T. Revealed Architectures of Adsorbed Polymer Chains at Solid-Polymer Melt Interfaces. *Phys. Rev. Lett.* **2012**, *109*, 265501.
(29) Bal, J. K.; Beuvier, T.; Unni, A. B.; Chavez Panduro, E. A.; Vignaud, G.; Delorme, N.; Chebil, M. S.; Grohens, Y.; Gibaud, A. Stability of Polymer Ultrathin Films (<7 nm) Made by a Top-Down Approach. *ACS Nano* **2015**, *9*, 8184−8193.
(30) Martínez-Tong, D. E.; Vanroy, B.; Wübbenhorst, M.; Nogales, A.; Napolitano, S. Crystallization of Poly($_L$-lactide) Confined in Ultrathin Films: Competition between Finite Size Effects and Irreversible Chain Adsorption. *Macromolecules* **2014**, *47*, 2354−2360.

DOI: 10.1021/acs.jpclett.6b02573
J. Phys. Chem. Lett. 2017, 8, 229−234